Chronic dosing of a simulated pond ecosystem in indoor aquatic mesocosms: Fate and Transport of CeO2 nanoparticles

Journal:	*Environmental Science: Nano*
Manuscript ID:	EN-ART-04-2015-000092.R2
Article Type:	Paper
Date Submitted by the Author:	25-Aug-2015
Complete List of Authors:	Tella, Marie; CEREGE UMR7330 CNRS Aix Marseille Universite, Interfast Auffan, Melanie; CEREGE UMR7330 CNRS Aix Marseille Universite, Interfast Brousset, Lenka; IMBE, Morel, Elise; CEREGE UMR7330 CNRS Aix Marseille Universite, Interfast proux, olvier; OSUG, Chaneac, Corinne; LCMCP, Material Chemistry Angeletti, Bernard; CEREGE UMR7330 CNRS Aix Marseille Universite, Interfast Pailles, Christine; CEREGE UMR7330 CNRS Aix Marseille Universite, Interfast Artells, Ester; Aix-Marseille Université, ; IMBE, Santaella, Catherine; Laboratoire d'Ecologie Microbienne de la Rhizosphere & Environnement Extrêmes, CNRS-CEA-Aix-Marseille Université Rose, Jérôme; CEREGE UMR7330 CNRS Aix Marseille Universite, Interfast Thiery, Alain; Université Marseille, IMBE - CNRS UMR 7263, Marseille France., Bottero, Jean-Yves; CEREGE UMR7330 CNRS Aix Marseille Universite, UMR 6635 CNRS/Aix Marseille University

SCHOLARONE™
Manuscripts

Nano Impact Statement

Current strategies to assess the environmental safety of engineered nanomaterials are based on classical ecotoxicology approaches, which are not always adequate. Indeed, while the hazard is extensively investigated, little attention is paid to the exposure to nanomaterials despite its pivotal role in understanding their environmental risks. Indoor aquatic mesocosms were designed to mimic pond ecosystems contaminated by a continuous point-source discharge of CeO_2 nanoparticles. Geochemical modeling was combined with chemical analysis, time-resolved laser diffraction, and high-energy resolution fluorescence detected X-ray absorption spectroscopy to adequately monitor the exposure of benthic and planktonic organisms in these mesocosms.

Environmental Science: Nano

ARTICLE

Chronic dosing of a simulated pond ecosystem in indoor aquatic mesocosms: Fate and Transport of CeO$_2$ nanoparticles

M. Tella[a,b], M. Auffan*[a,b], L. Brousset[b,c], E. Morel[a], O. Proux[d], C. Chanéac[b,e], B. Angeletti[a,b], C. Pailles[a,b], E. Artells[b,c], C. Santaella[b,f], J. Rose[a,b], A. Thiéry[b,c], J-Y. Bottero[a,b]

Indoor aquatic mesocosms were designed to mimic pond ecosystems contaminated by a continuous point-source discharge of cerium oxide nanoparticles (CeO$_2$-NPs). Bare and citrate-coated CeO$_2$-NPs exhibited different chemical and colloidal behaviors in the aquatic mesocosms. Bare CeO$_2$-NPs were chemically stable but quickly homo-aggregated and settled out of the water column, whereas citrate-coated NPs both homo- and hetero-aggregated but only after the several days required to degrade the citrate coating. While more stable as a colloidal suspension, coated CeO$_2$-NPs dissolved due to surface complexation with citrate, which resulted in the release of dissolved Ce into the water column. The different distributions over time between water/sediments or dissolved/particulate forms of Ce controlled the availability of Ce to benthic grazers (mollusk *Planorbarius corneus*) *and* planktonic filter feeders (copepod *Eudiaptomus vulgaris*).

Environmental Science: Nano

RSC**Publishing**

ARTICLE

1 ## Introduction

2 The current global production of cerium oxide nanoparticles (CeO_2-NPs) is estimated to be ~10 000 tons [1], with major CeO_2-NP

3 producers located in Asia, Australia, and Europe. The primary industrial sectors in which CeO_2-NP technology is expected to be

4 employed are electronics and optics, catalysts, energy and environment, coatings and paints [2]. Park et al. (2008) projected that

5 1255 tons of CeO_2 could be used in diesel fuel alone in the European Union in the year 2020 [3]. Collin et al. (2014) estimated that

6 adding CeO_2 to fuels could lead to a global CeO_2 consumption of 4 400 tons/year, and 15-25% of CeO_2 in fuel additives is

7 expected to be present as nanoparticles [4]. Keller et al. (2013) further estimate that 8 200 tons/year of CeO_2 might be released to

8 landfills, 1 400 tons/year to soils, 100 tons/year to air, and 300 tons/year to water [2]. Once released into natural environments, the

9 physico-chemical behavior of CeO_2-NPs will depend on environmental conditions (*e.g.* salinity, pH, dissolved organic matter,

10 natural colloids), nanoparticle properties (*e.g.* size, coating), and conditions within the product life cycle (*e.g.* formulation, use, end

11 of life), all of which will govern exposure of organisms (*e.g.* micro- and macro-organisms, benthic and planktonic organisms) to

12 CeO_2-NPs.

13 To date, the thorough characterization of the colloidal and chemical stability of nanoparticles in the presence of biota and natural

14 colloids at relevant concentrations over long periods of time remains challenging [5], but a few studies have attempted to make

15 headway in this area. One such study [6] focused on the exposure and environmental impact of a 1 mg.L^{-1} pulse dose of CeO_2-NPs

16 (4-nm) released to a simulated pond ecosystem. The authors successfully identified interactions between the nanoparticles and

17 naturally occurring (in)organic colloids and determined the distribution of CeO_2-NPs and dissolved Ce among the different

18 compartments of the simulated ecosystem (aqueous □phase, sediments, biota). However, information is still needed regarding the

19 role of particle size and coating on the aggregation and dissolution mechanisms and kinetics in this particular system. Moreover,

20 Auffan et al. (2014) showed that the chosen contamination scenario (whether as runoff from rain or vent loading [*i.e.,* single

21 pulse], or as a wastewater treatment plant or industrial discharge [*i.e.,* continuous or multiple dosing]) strongly controls persistence

22 of nanoparticles in the water column and uptake by organisms [5]. In the present study, we combine indoor aquatic mesocosms (*i.e.,*

23 the simulated pond ecosystem) with geochemical modeling, time-resolved laser diffraction, and high-energy resolution

24 fluorescence detected X-ray absorption spectroscopy to adequately monitor the exposure of benthic and planktonic organisms to

25 CeO_2-NPs during a continuous point-source discharge. Bare CeO_2-NPs and citrate-coated CeO_2-NPs available commercially as

26 wood-stain adjuvant were used as potential contaminants to a simulated pond trophic system comprising primary producers (algae,

27 bacteria) and primary consumers (mollusk *Planorbarius corneus* and copepod *Eudiaptomus vulgaris*). The chemical and colloidal

28 stability of CeO_2-NPs were thoroughly characterized, and the implications for uptake by benthic and planktonic organisms were

29 investigated.

30

31 ## Materials & Methods

32 ### CeO_2 nanoparticle characteristics

33 Two commercially available types of CeO_2-NPs (bare and citrate-coated crystallites of cerianite) were used in this study. The bare

34 CeO_2-NPs (Nanograin®, Umicore) had a primary particle size of 31 ± 18 nm (determined using TEM; see SI), an average

35 hydrodynamic diameter centered around 90 nm and zeta potential of 42 ± 2 mV in the stock suspension (in ultrapure water at

36 pH=3.1), and an isoelectric point (IEP) of pH~7.8 ± 2. Citrate-coated CeO_2-NPs (Nanobyk3810®, Byk), sold as long-term UV-

37 stabilizers were thoroughly described in Auffan et al. (2014) [7]. Briefly, the citrate-coated CeO_2-NPs had a primary particle size of

38 3.9±1.8 nm (determined using TEM; see SI), an average hydrodynamic diameter centered around 8 nm and a zeta potential of

39 -40±4 mV in ultrapure water from pH 3 to 10. The specific surface areas (SSA) are estimated as 56±10 $m^2.g^{-1}$ and 271±177 $m^2.g^{-1}$

40 for the 31-nm bare CeO_2-NPs and the 4-nm citrate-coated CeO_2-NPs, respectively. An additional batch of bare CeO_2-NPs with a

41 primary particle size of 3-4 nm, an average hydrodynamic diameter centered around 8 nm (in ultrapure water at pH=3.1), and an

42 IEP between pH 7 and 7.5 was also used during batch experiments [8].

Mesocosm set-up and monitoring

44 Nine indoor mesocosms (glass tanks of 750 × 200 × 600 mm) were set up to mimic a natural pond ecosystem. Natural sediments

45 and organisms were collected from a non-contaminated pond in the preserved Natura 2000 Reserve Network in southern France

46 (43.34361 N, 6.259663 E, altitude 107 m a.s.l.). Each mesocosm consisted of a layer of artificial sediment (79% SiO_2, 20%

47 kaolinite, 1% $CaCO_3$) covered with 300 g of water-saturated natural sediment containing primary producers (*e.g.,* algae, bacteria),

48 and 46 L of Volvic® water with pH and conductivity values close to those of natural pond water. See Auffan et al. (2014) [5] for

49 more details on the mesocosm set-up and monitoring. Three weeks of equilibration were necessary for the stabilization of the

50 physico-chemical parameters (pH, oxidation-reduction potential [ORP], dissolved O_2, and turbidity) in the mesocosms and the

51 development of the primary producers. After the equilibration period, 11 mollusks (*P. corneus* (L. 1758), benthic grazers) and 200

52 copepods (*E. vulgaris* (S. 1896), planktonic filter feeders) were introduced to each mesocosm. The organism density and

53 male/female ratio were selected according to the natural biotope. Starting at Day 0 (2 days after introduction of the organisms to

54 the mesocosms), the water columns were dosed 3 times per week (on Monday, Wednesday, and Friday) for 4 weeks with 5.2 mg

55 of CeO_2-NPs until Day 28, resulting in a final concentration of 1.1 mg.L^{-1} CeO_2-NPs and a total CeO_2 mass of 52.7 mg in the

56 mesocosms. Three mesocosms were dosed with bare CeO_2-NPs, three with citrate-coated CeO_2-NPs, and three were kept as

57 controls.

58 Details on the parameters monitored during the 7-week experiment are provided in the SI and Auffan et al. (2014) [5]. Briefly,

59 temperature (25.3 ± 0.6ºC), dissolved O_2 (7.4±0.5 mg.L^{-1}), pH (7.9±0.1), and total organic carbon (2.0±0.1 mg.L^{-1}) were constant

60 over time. ORP probes indicated that the water column was oxidative (241±10 mV), while reductive conditions prevailed in

61 sediments (-267±15 mV). Conductivity increased during the experiment from 293±8 µS.cm^{-1} to 318±15 µS.cm^{-1} due to weekly

62 refills with Volvic® water to compensate for evaporation. The concentration of phosphates and carbonates were 3.8×10^{-6} mol.L^{-1}

63 and 0.2×10^{-3} mol.L^{-1}, respectively, in the control mesocosms after 4 weeks. The primary producers were counted weekly in both

64 the water column and sediments. The concentrations of picoplankton and algae were respectively between 10^4-10^5 cells.mL^{-1} and

65 <10^3 cells.mL^{-1} in the water column and between 10^6-10^7 cells.mL^{-1} and 10^5-10^6 cell.mL^{-1} at the surface of the sediments (see SI).

66 The concentration of particles ranging in size from 0.5 to 2.5 µm in the water column was 10^6 mL^{-1}, as measured using an optical

67 counter (HIAC).

Cerium quantification

69 The distribution of Ce in the mesocosms was quantified by measuring the Ce content in surficial sediments (depth of sampling

70 estimated at about 0.9±0.4 cm) [6], the water column (at ~10 cm from the air/water interface and ~5 cm from the water/sediment

71 interface), and in the organisms using ICP-MS (NexIon 300X, Perkin Elmer) or ICP-AES (Jobin-Yvon Horiba). Surficial

72 sediments and water were sampled at Days 0, 1, 2, 7, 14, 21, and 28. See Tella et al. (2014) [6] for experimental details about sample

73 digestion and ICP analysis. Organisms were sampled weekly; at least 10 copepods from each mesocosm were collected, dried, and

74 acid digested at each time point. The weight of the copepods from each time point was determined by biovolume measurements [9]

75 (see SI). Adult *P. corneus* were dissected and their digestive glands acid digested (2 mL HNO_3 and 1 mL H_2O_2) before ICP-MS

76 analysis. Each measurement was performed in triplicate, and the measurement quality was controlled using certified reference

77   materials (estuarine sediment BCR 667 and mussel tissues BCR 668 from IRMM). All Ce concentrations presented are
78   expressed in mg.kg^{-1} dry weight.

Cerium speciation

80   X-ray Absorption Near Edge Structure (XANES) measurements were performed at the Ce L$_3$-edge on the CRG-FAME beamline
81   at the ESRF (Grenoble, France) on water column and surficial sediment samples from Day 28 of the experiment. For the water
82   column, 6 L of water was ultracentrifuged (396 750 g for 1h), and the solid phase was freeze-dried. Spectral acquisition was
83   performed at liquid helium temperature on freeze-dried samples to avoid sample evolution under the beam. Measurements were
84   carried out in fluorescence mode using a Canberra Ge solid-state detector or a crystal analyzer spectrometer (see SI) [10, 11]. Each
85   spectrum was at least the sum of three scans. The data reduction was performed using an Ifeffit software package [12]. Initial bare
86   and citrate-coated CeO$_2$-NPs and Ce^{III}-cysteine were used as Ce^{IV} and Ce^{III} reference samples. Ce^{III}-cysteine was laboratory-
87   synthetized (equimolar solution of Ce(SO$_4$)$_2$ and L-cysteine at pH=1) [13].

CeO$_2$-NPs solubility

89   Dialysis bags (10 KDa) were placed in the water column of the mesocosms to assess CeO$_2$-NP dissolution during the experiment.
90   In addition, bare and coated CeO$_2$-NP suspensions were diluted to 1 mg.L^{-1} in Volvic$^®$ water at pH 8 to study NP solubility in
91   batch experiments. Bare CeO$_2$-NPs were diluted in 10^{-2} and 10^{-3} mol.L^{-1} citrate solutions to assess the role of the citrate coating on
92   CeO$_2$-NPs dissolution. From 6 hours to 2 days, these suspensions were periodically ultrafiltered (Amicon tubes, 3KDa) and
93   dissolved Ce in the filtrate was measured by ICP-MS. The pH was monitored throughout the 2-day experiment.

Geochemical modeling of cerium speciation in the water column

95   Geochemical calculations were performed using the MEDUSA code [14] to predict phases that predominate in the pH and Eh range
96   of the mesocosm water columns. Diagrams of phase predominance of Ce were built with the aim of describing the equilibrium
97   state of CeO$_2$-NPs in natural aqueous environments. The fixed activities of Ce and other components in the water column were
98   used as input data.

CeO$_2$-NP homo- and hetero-aggregation

100   The initial size distribution and hetero-aggregation state of the kaolinite suspensions in Volvic$^®$ water in the presence of CeO$_2$-NPs
101   (1 mg.L^{-1}) were measured by laser diffractometry using the Mastersizer 3000 (Malvern, UK) in batch experiments. The
102   concentration of kaolinite (20 mg.L^{-1}; ~ 6×10^7 particles.mL^{-1} between 0.5 and 2.5 μm) was chosen to be close to the number of
103   particles in the water column of the mesocosms and in the detection range of the apparatus. Experiments were carried out in a
104   system of well-controlled hydrological conditions in a 1L beaker connected with plastic tubing to the measurement cell of the laser
105   diffractometer. The experimental suspension was continuously pumped through the system at a constant rate of ~100 mL.min^{-1};
106   the tubing was kept as short as possible to ensure reproducible conditions between different experiments and minimize the effect
107   of shear in the tube on the aggregation kinetics of the system [15]. Data are expressed in DV$_{50}$ values that represent the volume-
108   weighted median particle size. Homo-aggregation of the CeO$_2$-NP suspensions was also studied at 10 mg.L^{-1} (concentration
109   allowing for good detection) in Volvic water$^®$ using the NanoZS (Malvern, UK) and the Mastersizer 3000 (Malvern, UK) in batch
110   experiments. Homo- and hetero-aggregation experiments were performed under daylight conditions at ambient temperature.
111

Results & discussion

Colloidal behavior of CeO$_2$-NPs in mesocosms

114   **Distribution between the water column and the surficial sediments.** Surface and deep waters were sampled 1h30, 3h, 6h, 24h,
115   and 48h after the first injection of 5.2 mg of CeO$_2$-NPs (*i.e.* a Ce concentration of 100 μg.L^{-1}) in each mesocosm. For bare CeO$_2$-

116 NPs, a concentration gradient between the top (9.9 ± 0.9 $\mu g.L^{-1}$ at ~10 cm from the air/water interface) and the bottom of the water

117 column (3 ± 1 $\mu g.L^{-1}$ at ~5 cm from the water/sediment interface) was observed after 1h30 (Figure 1a), after which the Ce

118 concentration between the top and the bottom of the water column did not significantly evolve. 93 ± 3 % of the Ce initially

119 introduced at the top of the water column settled out of the water column after 48h. For the coated CeO$_2$-NPs (Figure 1b), an

120 homogeneous Ce distribution (71 ± 12 $\mu g.L^{-1}$) between the top and the bottom of the water column was reached after 6 hours. Only

121 29 ± 12 % of the Ce initially introduced had settled out after 48h. These results highlight that waiting 2 to 3 days between each

122 dosing of NPs was enough to reach a steady state in terms of distribution in the water column.

123 After 4 weeks (Figure 2) the total Ce concentration in the water column remained stable at 5 ± 2 $\mu g.L^{-1}$ and 49 ± 7 $\mu g.L^{-1}$ for bare

124 and citrate-coated CeO$_2$-NPs, respectively. While the Ce concentration in the water column was ten times higher for the coated

125 NPs than for the bare NPs, similar Ce concentrations were measured in the surficial sediment for both types of CeO$_2$-NPs. The

126 concentration in the sediment reached 99 ± 42 $mg.kg^{-1}$ after 4 weeks with a sedimentation rate of 1.0 ± 0.1 mg per day, which

127 corresponds to ~99% (bare NPs) and ~75% (coated NPs) settling of Ce injected after 28 days. These percentages are in agreement

128 with previous studies simulated using a single-pulse input of CeO$_2$-NPs [6, 16] or Ag-NPs [17] in mesocosms. The factor of ~10

129 difference in the concentration of Ce in water after dosing with bare *versus* coated CeO$_2$-NPs – and the longer time needed to

130 obtain a homogeneous distribution of Ce in the water column for the coated CeO$_2$-NPs – highlight different colloidal behaviors

131 between these types of CeO$_2$-NPs (Figure 1 and 2).
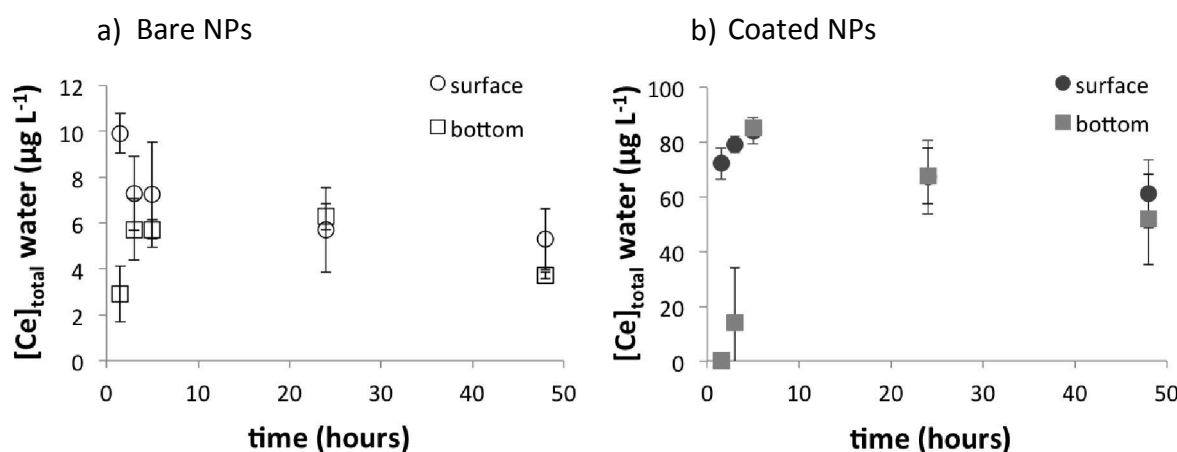
132

133 Figure 1. Short-term distribution of cerium in the water column after the first input of 5.2 mg of bare cerium oxide nanoparticles (CeO$_2$-NPs) (a) and coated CeO$_2$-NPs

134 (b). Water was sampled at ~10 cm from the air/water interface and at ~5 cm from the water/sediment interface. Data represent average ± standard deviation of

135 triplicates and are corrected from background concentration determined in control mesocosms.

136
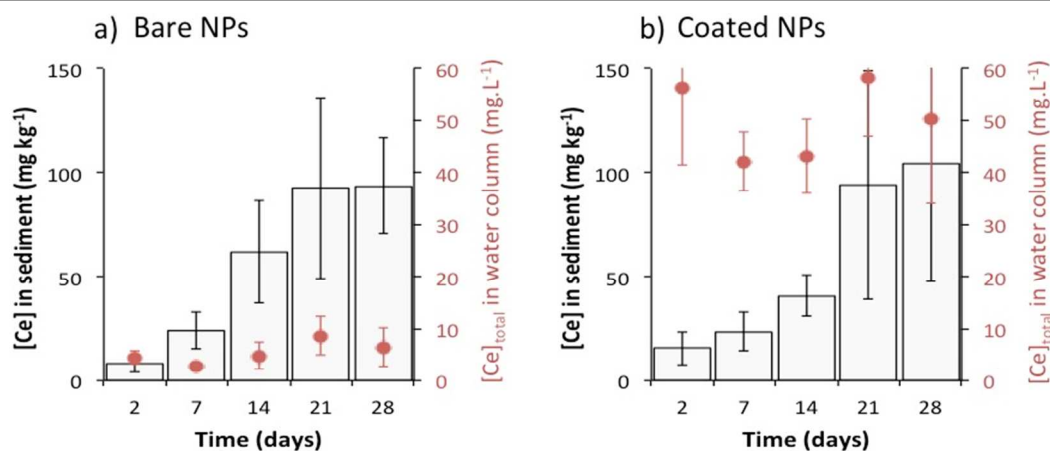
Figure 2. Long-term distribution of Ce between the water column and the surficial sediments after 28 days of CeO$_2$-NPs contaminations. (a) bare CeO$_2$-NPs and (b) coated CeO$_2$-NPs. Water was sampled at ~10 cm from the air/water interface. Data represent the average of three replicates ± standard deviation and are corrected from background concentration determined in control mesocosms.

Homo-aggregation *versus* hetero-aggregation. Aggregation between particles can be modelled by the Smoluchowski equation (1917) [18] :

$$dn / dt = -\alpha\beta(n, B)nB + K_B(n_0 - n)$$

with β as the product of the second-order collision rate constant, n as the concentration of un-hetero-aggregated NPs, B as the concentration of background particles, and α as the affinity coefficient between nano- and background particles. The reverse reaction (breakup of larger aggregates into the primary particle sizes) can be assumed to be proportional (by the breakup rate constant K_B) to the number of NPs that have hetero-aggregated $(n_0 - n)$. Recent work on homo- and hetero-aggregation have elucidated methods for distinguishing between α due to the two aggregation processes [15, 19-21]. In the present study, changes in hydrodynamic diameters as a function of time were monitored to evaluate early-stage aggregation in both the homo- and hetero-aggregation scenarios.

Homo-aggregation was assessed in Volvic® water at pH 8 in batch experiments (Figure 3). Bare CeO$_2$-NPs homo-aggregated in a few minutes and achieved an average hydrodynamic diameter of a few tens of microns within 4h, whereas coated CeO$_2$-NPs remained more stable, with an average size below 1 μm after 180 hours (Figure 3) [6]. The faster homo-aggregation of the bare CeO$_2$-NPs can be explained by the IEP of these particles (at pH=7.8±2), which is close to the pH of the Volvic® water. The zeta potentials of the bare CeO$_2$-NPs measured under these pH and ionic strength conditions were about -2.6±0.8 mV at 0.1h and 5±3 mV at 4.5h. Based on Stokes law, homo-aggregates of bare CeO$_2$-NPs with an average size of 30 μm would require less than 10 min to settle out in the mesocosm set-up, which is consistent with the fast kinetics of sedimentation of bare NPs measured by chemical analysis of the sediment (Figure 1). However, the kinetics of homo-aggregation of the coated CeO$_2$-NPs were slower, likely due to the negatively charged coating that prevents homo-aggregation (Figure 3). The zeta potentials of the coated CeO$_2$-NPs measured under these pH and ionic strength conditions evolved from -14±4 mV at 0.1h to 1±0.1 mV at 180h. Auffan et al. (2014) [7] demonstrated that citrate forms a chelate with Ce^{IV} through its central carboxyl- and α-hydroxyl- groups at the surface of the CeO$_2$-NPs. In the mesocosms, the citrate coating is degraded over time due to *(i)* strong dilution, which changes the chemical equilibrium and favors the citrate desorption and (ii) to the presence of daylight that favors citrate degradation into acetate, oxalate, and other degradation by-products. Auffan et al. (2014) [7] measured an IEP of pH=6±1 for citrate-coated CeO$_2$-NPs after citrate degradation [7]. Consequently, the slow citrate-coated CeO$_2$-NP homo-aggregation observed in Volvic® water was likely due to degradation of the citrate coating [6, 7].

168

169
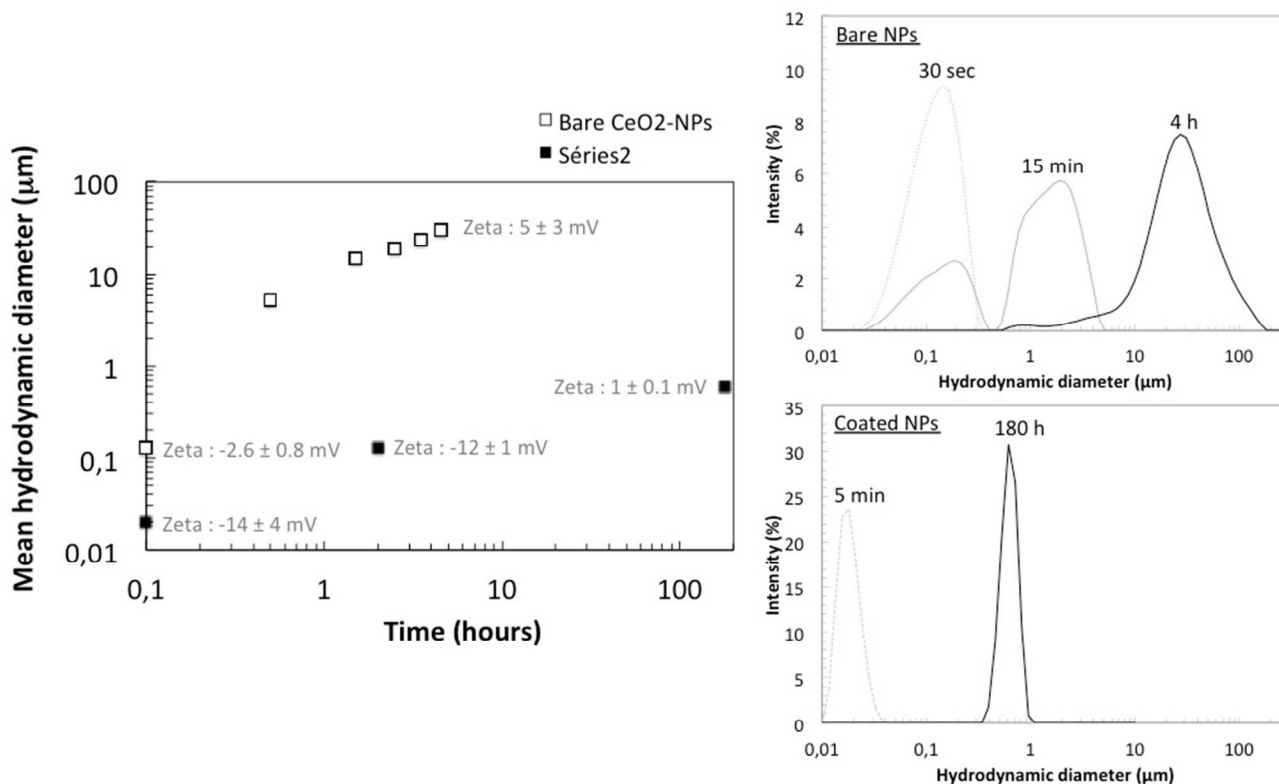
170   Figure 3. Homo-aggregation of bare and citrate-coated cerium oxide nanoparticles (CeO$_2$-NPs) in Volvic® water at 10 mg.L^{-1} in batch experiments. Zeta potential
171   measurements were performed in Volvic® water (pH 7.9±0.1).

172

173   Natural colloids present in the mesocosm water (*e.g.* suspended clays, natural organic matter) can also cause settling out of NPs
174   through hetero-aggregation [6, 15, 22, 23]. In the mesocosms, the number of colloids (mostly kaolinite particles) was close to 10^6
175   particles.mL^{-1}, the number of bare CeO$_2$-NPs (31±18 nm) between 10^9 particles.mL^{-1} (for 0.1 mg.L^{-1}) and 10^{10} particles.mL^{-1} (for
176   1.1 mg.L^{-1} at Day 28), and the number of coated CeO$_2$-NPs (3.9±1.8 nm) between 5×10^{11} particles.mL^{-1} (for 0.1 mg.L^{-1}) and
177   5×10^{12} particles.mL^{-1} (for 1.1 mg.L^{-1} at Day 28). The interactions between kaolinite and bare or coated CeO$_2$-NPs were studied by
178   time-resolved laser diffraction in Volvic® water at pH=7.9 in batch experiments. Under these conditions, kaolinite particles form
179   stable homo-aggregates at about 16-17 µm (DV$_{50}$; see SI). After the injection of 1 mg.L^{-1} CeO$_2$-NPs, a significant modification of
180   the DV$_{50}$ of the kaolinite occurred only with the 4-nm bare CeO$_2$-NPs (increase of ~4.3 µm) and not with 31-nm bare or 4-nm
181   coated CeO$_2$-NPs (Figure 4 and 5). Therefore, hetero-aggregation seems to be active only for small-sized bare NPs in conjunction
182   with homo-aggregation. Figures 4 and 5 also highlight that the degradation of the citrate present at the surface of the coated NPs
183   needs to be taken into account for hetero-aggregation [6, 7]. Indeed, coated CeO$_2$-NPs were aged 3 days under daylight in Volvic®
184   water (see ref [6, 7] for details) and were exposed to kaolinite particles. The aged, coated NPs destabilized the kaolinite suspension 20
185   min after injection, with an increase of the DV$_{50}$ by ~5 µm (Figure 5). It is noteworthy that the aged, coated NPs have a zeta
186   potential close to that of the bare NPs [7], but the bare NPs did not hetero-aggregate with the clays. The main difference between the
187   two types of NPs is the primary particle size: 31±18 nm for bare *versus* 4±1 nm for aged, coated CeO$_2$-NPs. The difference in
188   primary particle size of the two particles consequently affects the respective particle numbers in suspension (10^{10} particles.mL^{-1}
189   and 5×10^{12} particles.mL^{-1} for the 31-nm bare and the 4-nm aged, coated CeO$_2$-NPs, respectively). The ratio of NPs to kaolinites
190   was determined to be ~ 500 times lower for bare CeO$_2$-NPs than for aged, coated CeO$_2$-NPs (based on the number of kaolinite

191 particles between 0.5 and 2.5 μm of 6×10^7 particles.mL^{-1}); this difference in availability of particle surfaces to interact with sites at

192 the surface of the clays would be expected to result in a difference in the fate of two types of CeO$_2$-NPs. Kaolinite is a 1:1-type

193 aluminosilicate clay [(Si$_4$)^{IV}(Al$_4$)^{VI}O$_{10}$(OH)$_8$] in which one tetrahedral sheet is combined with one octahedral sheet, forming a layer

194 stack. This structure results in a crystal with a siloxane basal surface, an alumina basal surface with >Al$_2$OH groups, and lateral

195 surfaces with silanol (>SiOH) and aluminol (>AlOH) groups [24]. The charges of these lamellar particles are localized on the lateral

196 surfaces [25] and can act as deposition sites that alter the fate of NPs in most aquatic systems. Based on Sayed Hassan et al. (2005)

197 [26], the average specific surface area of kaolinites is estimated at about 24 m^2.g^{-1}, with 19 m^2.g^{-1} attributed to basal faces and 5 m^2.g$^-$

198 ^{1} to lateral faces. Assuming that CeO$_2$-NPs interact specifically with the more reactive lateral surfaces, we estimate that 20 mg.L^{-1}

199 of kaolinite correspond to 0.10 m^2.L^{-1} of lateral surface available to interact with the 0.03 m^2.L^{-1} of 31-nm bare NPs and the 0.2

200 m^2.L^{-1} of 4-nm aged coated NPs. The partial coating of lateral faces of kaolinite by CeO$_2$-NPs is then more favorable for 4-nm

201 aged coated NPs than for the 31-nm bare NPs. The chemical mechanism of hetero-aggregation at pH=7.9 is related to the sorption

202 of CeO$_2$-NPs through Ca^{2+} ion bridges between the negative lateral charges of kaolinite [25] and the neutral surfaces of the 4-nm

203 bare CeO$_2$-NPs or the negative surfaces of the aged coated CeO$_2$-NPs [7].

204 To conclude, two aggregation mechanisms co-occurred in the water column of the mesocosms. For 31-nm bare CeO$_2$-NP, homo-

205 aggregation appears to be the most favorable mechanism; these particles settled out very quickly due to the relative number of

206 particles in suspension and particle surface charges. For coated CeO$_2$-NPs, both homo-aggregation and hetero-aggregation were

207 favorable, but a few days were required under artificial daylight to degrade the citrate coating in the water column.

208

209

210
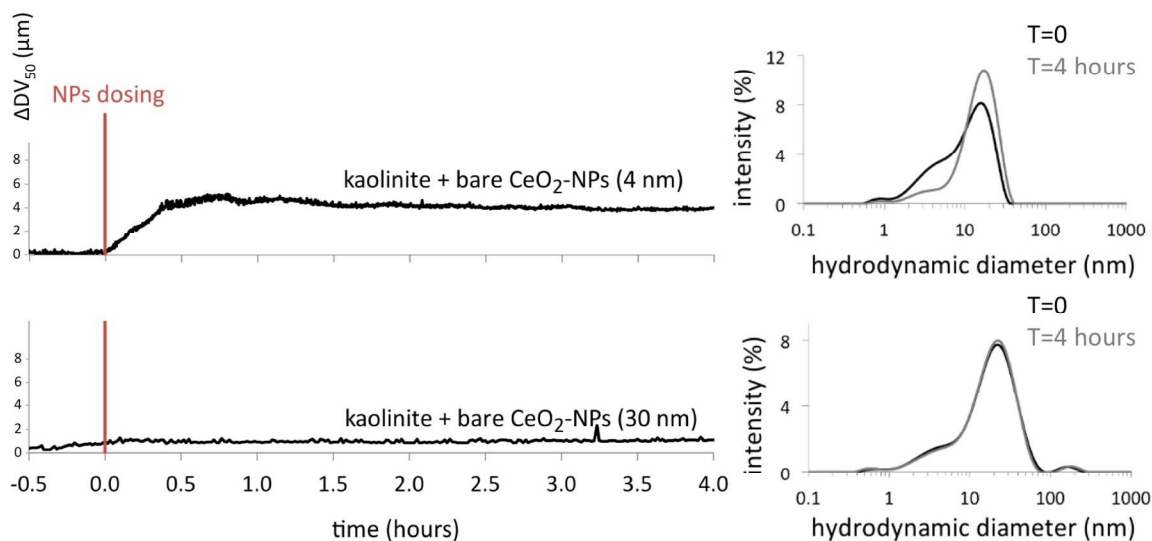
Figure 4. Hetero-aggregation of bare cerium oxide nanoparticles (CeO_2-NPs) (~4 nm and ~31 nm) with kaolinite during batch experiments. Red line indicates the injection of 1 mg.L^{-1} of NPs in the kaolinite suspension (20 mg.L^{-1}) in Volvic® water. Data are expressed in ΔDV_{50} *i.e.* the volume-weighted median particle size at a given time subtracted from the volume-weighted median particle size of the kaolinite 30 min before NPs dosing.

214
215
216

217

218

Figure 5. Hetero-aggregation of initial and aged coated cerium oxide nanoparticles (CeO_2-NPs) with kaolinite during batch experiments. Red line indicates the injection of 1 mg.L^{-1} of NPs in the kaolinite suspension (20 mg.L^{-1}) in Volvic® water. Data are expressed in ΔDV_{50} *i.e.* the volume-weighted median particle size at a given time subtracted from the volume-weighted median particle size of the kaolinite 30 min before NP dosing.
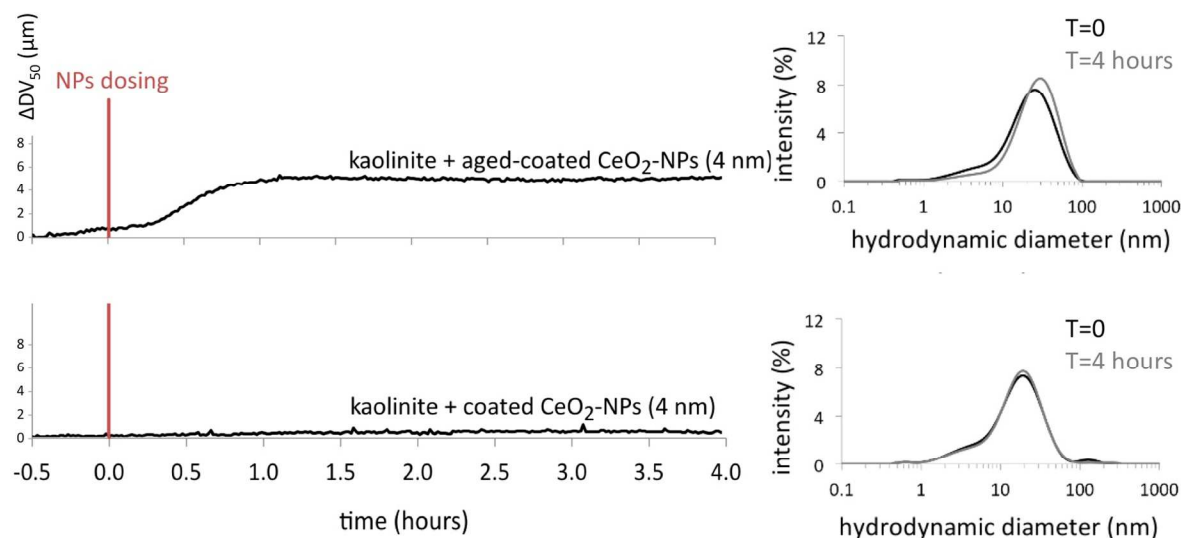
221
222

223   **Chemical behavior of CeO$_2$-NPs in mesocosms**

224   **CeO$_2$-NP solubility in the water column.** The concentration of dissolved Ce (<10 KDa) was measured in the water column of the

225   mesocosms weekly over 28 days. The dissolved Ce concentration stabilized after 2 days at 1.1±0.2 µg.L^{-1} for bare (Figure 6a) and

226   18±2 µg.L^{-1} for citrate-coated CeO$_2$-NPs (Figure 6b), which corresponds respectively to 22±4% and 36±5% of the total Ce

227   introduced. The strong chemical stability of bare CeO$_2$-NPs in the water column was also confirmed by XANES at the Ce L$_3$-edge

228   at which Ce^{III} was not detected (see SI). For both types of CeO$_2$-NPs, the concentrations of dissolved Ce measured in the

229   mesocosms were not in agreement with the low solubility expected for Ce oxy-hydroxide (K$sp_{Ce(OH)3}$ = 6.3×10^{-24} at 25°C [27]),

230   which suggests the presence of soluble inorganic or organic complexes of Ce in the mesocosms. The Ce speciation in the water

231   column was geochemically modeled considering the amount of cations and anions present in Volvic$^®$ water and the concentrations

232   of phosphates and carbonates measured in the water column of the mesocosms. For bare CeO$_2$-NPs (Figure 6c) the results of

233   modeling are quantitatively in agreement with the Ce concentrations measured in the water column: Ce^{III}-CO$_3^+$ aqueous complexes

234   represent 20% of the total Ce (*i.e.* 0.9 µg.L^{-1}) in equilibrium with CeO$_2$(s) at pH=7.9. However, these Ce^{III}-CO$_3^+$ complexes were

235   not sufficient to account for the dissolved Ce measured in mesocosms dosed with coated CeO$_2$-NPs (Figure 6d). Another

236   parameter that needed to be taken into account was the concentration of citrate present in the stock suspension of the coated CeO$_2$-

237   NPs [6]. An estimated concentration of 1.3×10^{-4} mol.L^{-1} of citrate was introduced to the mesocosms during the injection of the

238   coated CeO$_2$-NPs. The Ce speciation was then modeled considering Ce^{III}-Cit^0 complexes, and the results obtained were

239   quantitatively in agreement with the Ce concentrations measured in the water column: Ce^{III}-Cit^0 aqueous complexes represent 70%

240   of the total Ce (34 µg.L^{-1}) in equilibrium with CeO$_2$(s) at pH=7.9.

241

242   **Role of citrate on CeO$_2$-NP chemical instability.** To support the hypothesis that organic complexation of Ce surface atoms with

243   citrate favors the dissolution of coated NPs in the mesocosms, batch experiments were carried out in Volvic$^®$ water. Bare CeO$_2$-

244   NPs were incubated for 48h with increasing concentrations of citric acid (0, 10^{-3}, and 10^{-2} mol.L^{-1}) at pH=8. In the absence of citric

245   acid, dissolved Ce concentrations never exceeded the background concentration of Ce in the Volvic$^®$ water (0.5±0.2 µg.L^{-1}). In the

246   presence of citrate, dissolved Ce concentrations rose to 76±8 µg L^{-1} and 121±14 µg.L^{-1} for the 10^{-3} mol.L^{-1} and 10^{-2} mol.L^{-1} citrate

247   solutions, respectively (Figure 7). The increase of dissolved cerium in the presence of higher concentrations of citrate is in

248   agreement with the formation of Ce^{III}-citrate complexes already observed [28]. All results demonstrated the presence of CeO$_2$(s) in

249   equilibrium with CeCO$_3^+$ for bare CeO$_2$-NPs and CeCit^0 for coated CeO$_2$-NPs in the water column of the mesocosms.
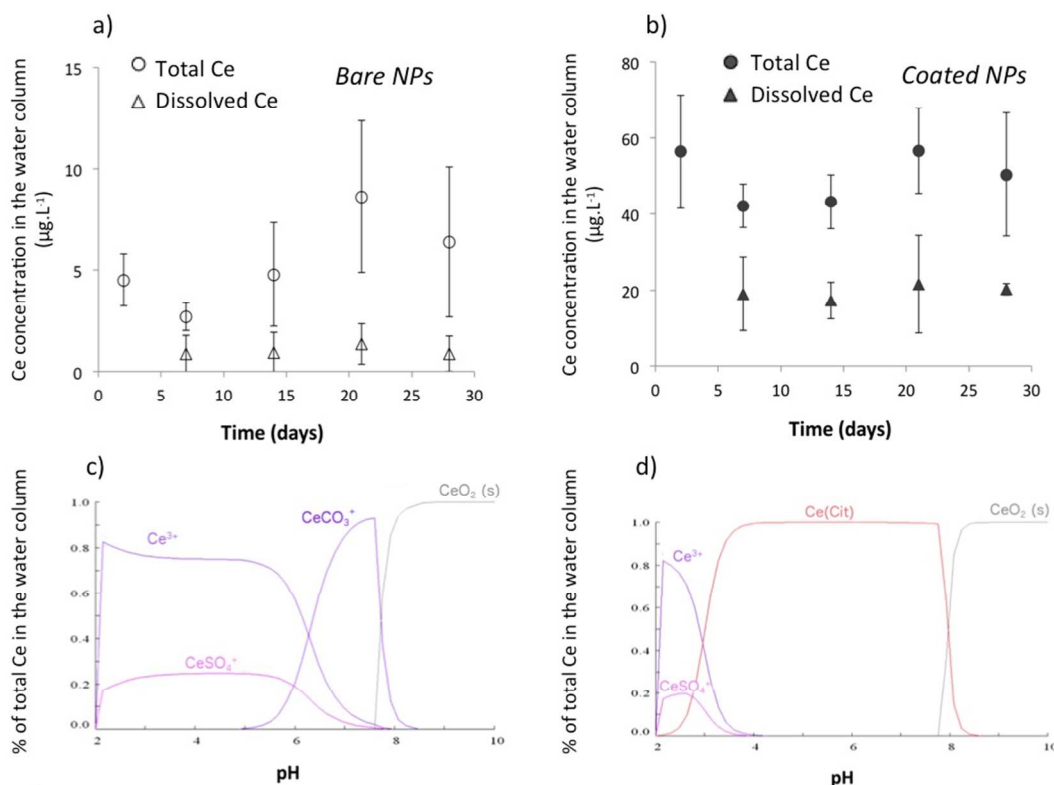
Figure 6. Cerium (Ce) concentrations (total and dissolved) in the water column of the mesocosms (a, b) and the corresponding modeling for the bare (c) and citrate-coated cerium oxide nanoparticles (CeO$_2$-NPs) (d). For total Ce measurements, water was sampled at ~10 cm from the air/water interface. For dissolved Ce measurements, water was sampled in dialysis bags (10 KDa) introduced into the mesocosms. The data are the average of three replicates ± standard deviation and are corrected from background concentrations determined in control mesocosms. See SI for the composition of the water column used for chemical modeling.
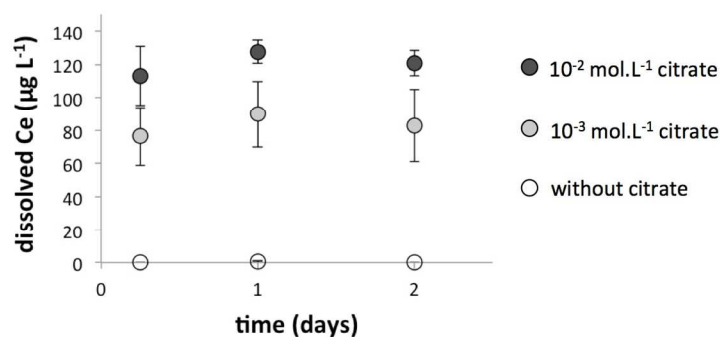
Figure 7. Influence of citrate on the solubility of cerium oxide nanoparticles (CeO$_2$-NPs). Batch experiments were carried out in Volvic® water with 1 mg.L^{-1} of bare CeO$_2$-NPs (31±18 nm). Dissolved cerium was measured after ultrafiltration of solutions at 3 KDa. Results indicate the average of three replicates ± standard deviation.

Speciation of cerium in surficial sediments. Previous results have shown that surficial sediments accumulated ~99% (bare NPs) and ~75% (citrate-coated NPs) of Ce injected after 28 days. The speciation (local order and valence) of the Ce accumulated in these sediments was studied by X-ray Absorption Spectroscopy (XAS) at the Ce L$_3$-edge. However, standard transmission or total fluorescence XAS spectra do not have the required energy resolution to unambiguously identify Ce^{III} in the structure of CeO$_2$ NPs [29]. HERFD-XAS (High Energy Resolution Fluorescence Detected XAS) could address this deficiency [30] by offering more defined

265   edges (Figure 8a) and pre-edges (Figure 8b) features for analysis. One of the most interesting features of HERFD-XAS is the ~2

266   eV difference between the pre-edges of Ce[III] and Ce[IV] reference compounds: 5719 eV for Ce[III] and 5721 eV for Ce[IV]. As shown in

267   Figure 8, the pre-edges of Ce in both samples were centered on 5721eV leading to the conclusion that no reduction of Ce[IV] into

268   Ce[III] occurred in the surficial sediments after 28 days in the mesocosms.

269

270
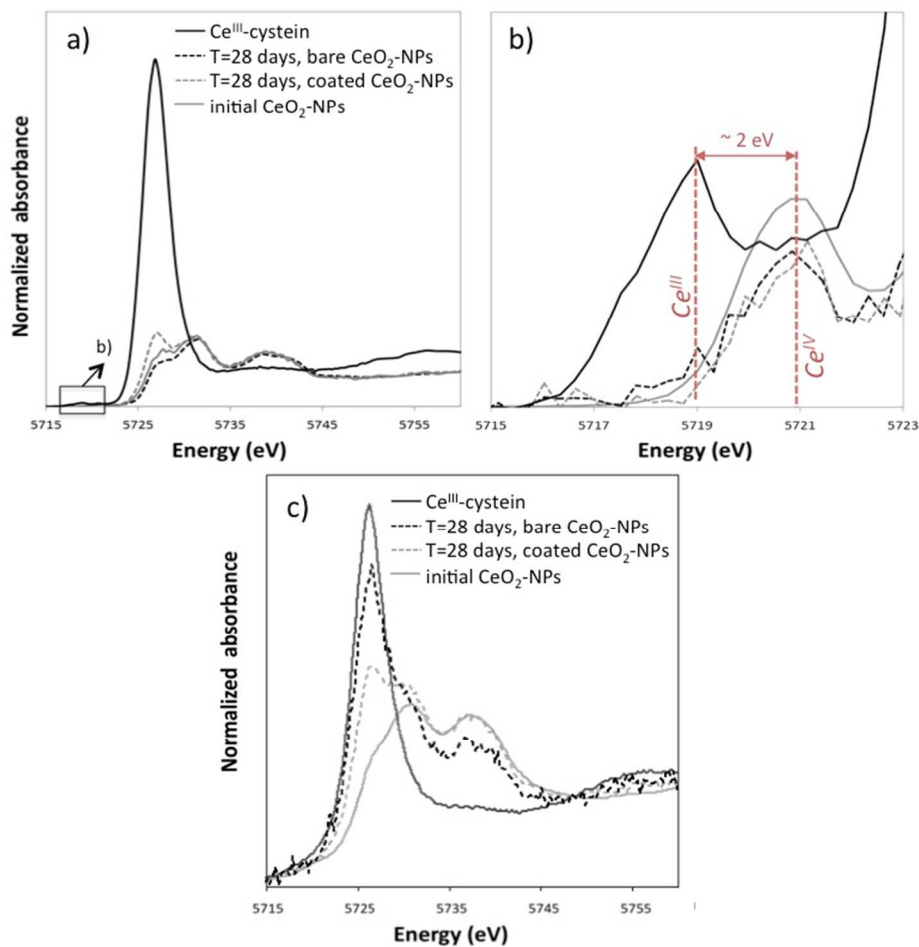
271   Figure 8. Cerium (Ce) L$_3$-edge X-ray Absorption Near Edge Structure (XANES) spectra of Ce accumulated on the surficial sediments (using High Energy Resolution

272   Fluorescence Detected XAS [HERFD-XAS]) (a, b) and in the digestive gland of *Planorbarius corneus* at day 28 (total fluorescence XAS) (c). Details of the pre-edge area

273   (b). Experimental spectra are compared to Ce[III]-cysteine and initial nanoparticle reference spectra.

274

275

276   **Implications of CeO$_2$-NP interactions with biota**

277

278   All data presented about the chemical and colloidal behaviors of CeO$_2$-NPs in aquatic mesocosms following a continuous point-

279   source discharge suggest drastically different fates for bare and citrate-coated CeO$_2$-NPs. Bare CeO$_2$-NPs quickly homo-

280   aggregated (Figure 3) and settled out (Figure 2), but were chemically more stable (Figure 6) than coated NPs, which dissolved

281   faster due to surface complexation with citrate (Ce[III]-Cit^0 complex, Figure 6 and 7). Moreover, coated CeO$_2$-NPs required a few

282   days of citrate-coating degradation before homo- and hetero-aggregation occurred (Figure 3 and 4).

283   Table 1 presents the concentrations of Ce taken up or adsorbed to the surface of *P. corneus* and *E. vulgaris* following exposure to

284   bare and citrate-coated CeO$_2$-NPs. *Eudiaptomus* are planktonic filter feeders that pass water currents through sieve- or comb-like

285   structures to feed [31, 32]. The Ce concentrations in the copepods (whole organism) after 2 weeks were 288±54 mg.kg^{-1} (dry weight)

286   and 3356±625 mg.kg^{-1} for bare and coated CeO$_2$-NPs, respectively. A similarly large amount was previously observed in daphnia

287   after exposure to 0.1 mg/L of TiO$_2$ NPs [33]. These planktonic filter feeders live and feed in the water column [32] and can ingest [34]

288   and adsorb [35] Ce on the cuticle. The longer persistence of Ce in the water column following dosing with citrate-coated NPs is in

289   agreement with the high amount of Ce measured in and/or on the surface of the copepods exposed to coated NPs. *Planorbarius* are

290   benthic grazers that feed on algae and biofilms at the sediment/water interface [36]. Consequently, the Ce concentration measured in

291   their digestive glands depends on the Ce concentration in the surficial sediments and the settling kinetics of homo- and hetero-

292   aggregates. The Ce concentration measured in whole *P. corneus* were not statistically different between bare (2.1±1.6 to 6.3±6.0

293   mg.kg^{-1}) and coated NPs (1.3±0.9 to 5.1±3.7 mg.kg^{-1}) over time (Table 1), which is in agreement with the lack of statistically

294   significant difference in Ce concentrations measured in surficial sediments.

295   In addition to ecological strategies, one important difference between *E. vulgaris* and *P. corneus* is the specific surface area (SSA)

296   available to adsorb Ce. The small size and large SSA of *E. vulgaris* could explain why the concentration in the whole copepods is

297   several orders of magnitude higher than in the whole *P. corneus* mollusks.

298   Biodistribution was also investigated using XANES at the Ce L$_3$-edge to analyze Ce speciation in the digestive glands of *P.*

299   *corneus* after 28 days. A significant reduction of Ce^{IV} to Ce^{III} was observed for both bare and coated-CeO$_2$ NPs in the digestive

300   glands (Figure 8c). A peak appeared on the XANES spectra for CeO$_2$-NPs at the energy of the edge observed for the Ce^{III}-cysteine

301   reference compound (Figure 8c). The intensity of the peak is higher for bare than coated CeO$_2$-NPs, highlighting a more important

302   bioreduction of Ce following bare CeO$_2$-NP ingestion. However, the XAS spectra acquired in total fluorescence do not have the

303   required energy resolution to quantitatively determine the percentage of Ce^{III} in the structure of the NPs [29].

304

305   Table 1. Concentration of cerium (Ce) (mg.kg^{-1} dry weight) measured in the whole planktonic *Eudiaptomus* copepods and on the digestive gland and whole
306   benthic *Planorbarius* mollusk exposed to cerium oxide nanoparticles (CeO$_2$-NPs over 28 days in mesocosms. For copepods, masses were estimated from
307   biovolumes considering 20% of dry matter in organisms. DG: digestive gland. N/A: Not analyzed.

308
309

	Bare CeO$_2$-NPs			**Coated CeO$_2$-NPs**		
	Planktonic	**Benthic**		**Planktonic**	**Benthic**	
	Whole	Whole	DG	Whole	Whole	DG
7 d	288±54	2.1±1.6	31±25	97±18	5.1±3.7	82±62
14 d	111±21	6.3±6.0	170±170	3356±625	1.6±1.1	16±18
21 d	N/A	4.4±4.1	140±130	N/A	1.3±0.9	9±8
28 d	N/A	2.8±N/A	85±N/A	N/A	3.4±2.4	60±42

310
311
312   **Conclusions**

313   The thorough characterization of the fate and transport of CeO$_2$-NPs presented in the current study highlights that the physico-

314   chemical mechanisms and kinetics of transformation and distribution will vary in complex ecosystems due to differences in the

315   size and surface properties of NPs but also on the kinetics and mechanisms of homo-aggregation, hetero-aggregation, Ce^{III}-organic

316   complexation, dissolution, and coating degradation. The degree to which these factors influences exposure and uptake of CeO$_2$-

317   NPs by organisms will also be determined by ecological strategies (*e.g.* benthic *versus* planktonic, filter feeders *versus* grazers)

318   (Figure 9), which suggests the need to further investigate significant differences in biological impacts on micro- and macro-

319   organisms with different ecological traits and strategies. In addition, this study was focused only on the first two links of a lentic

320   water trophic chain: the producers (diatoms, green algae, and biofilm) and the first consumers (filter feeders in the water column

321   and benthic grazers on sediments). For a better understanding of impacts on the food chain, the predators (*i.e.* secondary

322 consumers [*e.g.* dragonflies, water beetles]) should be investigated. Furthermore, the selected organisms were arbitrarily chosen at

323 the adult developmental stage. The fate of CeO_2-NPs in systems with newly hatched forms (*e.g.,* nauplius and copepodid phases

324 for copepods, shell-less gastropods) should be investigated.

325
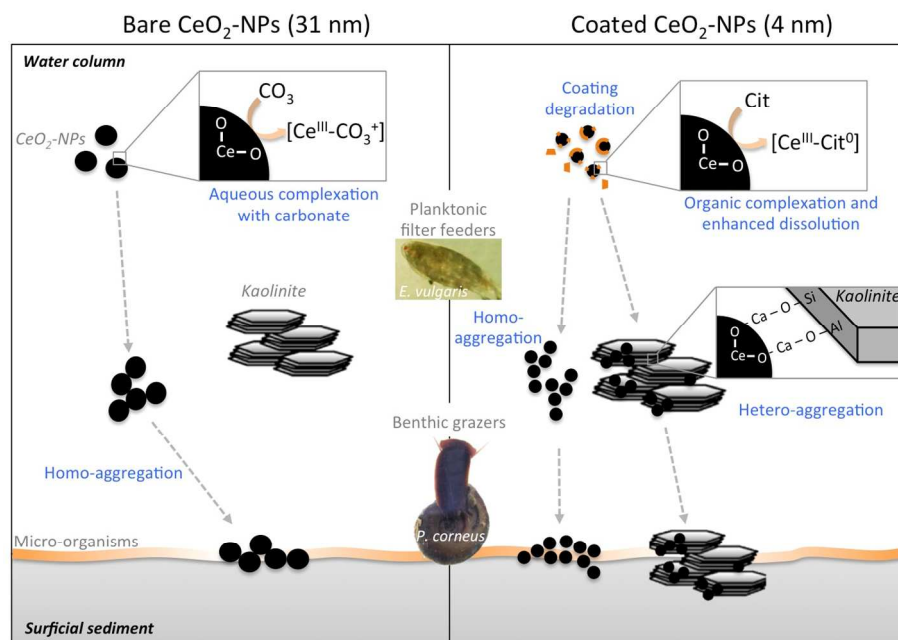
328 Figure 9. Scheme highlighting the physico-chemical mechanisms affecting the fate of cerium oxide nanoparticles in the mesocosms (*e.g.,* homo-aggregation, hetero-
329 aggregation, dissolution, complexation with organics, coating degradation) in relation to the ecological strategies of the organisms.

330

Acknowledgements

332

342

Notes and references

344 * Corresponding author

345 [a] CNRS, Aix-Marseille Université, CEREGE UM34, UMR 7330, 13545 Aix en Provence, France.

346 [b] International Consortium for the Environmental Implications of Nanotechnology iCEINT, Aix en Provence, France.

347 [c] Aix-Marseille Université/IMBE UMR 7263/Université Avignon, 13331 Marseille, France.

348 [d] Observatoire des Sciences de l'Univers de Grenoble, UMS 832, CNRS, Université Joseph Fourier, 38041 Grenoble, France

349 [e] UPMC Univ Paris 06, CNRS, UMR 7574, Chimie de la Matière Condensée de Paris, Collège de France, 75231 Paris, France

350 f CNRS, Aix-Marseille Université, CEA, IBEB, Cadarache DSV / IBEB / SBVME, Lab Ecol Microb Rhizosphere & Environ Extrem (LEMiRE),
351 UMR 7265, Saint Paul lez Durance, France

352

356

357 1.   European-Commission, 2012.
358 2.   A. Keller, S. McFerran, A. Lazareva and S. Suh, *Journal of Nanoparticle Research*, 2013, **15**, 1-17.
359 3.   B. Park, K. Donaldson, R. Duffin, L. Tran, F. Kelly, I. Mudway, J.-P. Morin, R. Guest, P. Jenkinson, Z. Samaras, M. Giannouli, H. Kouridis and P.
360   Martin, *Inhalation Toxicology*, 2008, **20**, 547 - 566.
361 4.   B. Collin, M. Auffan, A. C. Johnson, I. Kaur, A. A. Keller, A. Lazareva, J. R. Lead, X. Ma, R. C. Merrifield, C. Svendsen, J. C. White and J. M.
362   Unrine, *Environmental Science: Nano*, 2014, **1**, 533-548.
363 5.   M. Auffan, M. Tella, C. Santaella, L. Brousset, C. Pailles, M. Barakat, B. Espinasse, E. Artells, J. Issartel, A. Masion, J. Rose, M. Wiesner, W.
364   Achouak, A. Thiery and J.-Y. Bottero, *Scientific reports*, 2014, **4**, 5608.
365 6.   M. Tella, M. Auffan, L. Brousset, J. Issartel, I. Kieffer, C. Pailles, E. Morel, C. Santaella, B. Angeletti, E. Artells, J. Rose, A. Thiery and J.-Y.
366   Bottero, *Environmental Science & Technology*, 2014, **48**, 9004–9013.
367 7.   M. Auffan, A. Masion, J. Labille, M. A. Diot, W. Liu, L. Olivi, O. Proux, F. Ziarelli, P. Chaurand, C. Geantet, J.-Y. Bottero and J. Rose,
368   *Environmental Pollution*, 2014, **188**, 1-7.
369 8.   M. A. Diot, Aix-Marseille, 2012.
370 9.   J. Sun and D. Liu, *Journal of Plankton Research*, 2003, **25**, 1331-1346.
371 10.   J.-L. Hazemann, O. Proux, V. Nassif, H. Palancher, E. Lahera, C. Da Silva, A. Braillard, D. Testemale, M.-A. Diot, I. Alliot, W. Del Net, A.
372   Manceau, F. Gelebart, M. Morand, Q. Dermigny and A. Shukla, *Journal of Synchrotron Radiation*, 2009, **16**, 283-292.
373 11.   I. Llorens, E. Lahera, W. Delnet, O. Proux, A. Braillard, J.-L. Hazemann, A. Prat, D. Testemale, Q. Dermigny, F. Gelebart, M. Morand, A. Shukla,
374   N. Bardou, O. Ulrich, S. Arnaud, J.-F. Berar, N. Boudet, B. Caillot, P. Chaurand, J. Rose, E. Doelsch, P. Martin and P. L. Solari, *Review of
375   Scientific Instruments*, 2012, **83**, 063104.
376 12.   B. Ravel and M. Newville, *J. Synchrotron Radiat.*, 2005, **12**, 537-541.
377 13.   G.-C. Han, Y. Peng, Y.-Q. Hao, Y.-N. Liu and F. Zhou, *Anal. Chim. Acta*, 2010, **659**.
378 14.   I. Puigdomenech, in *219th ACS national meeting, Abstract of papers*, ed. A. C. Society, San Francisco, 2000, vol. 1.
379 15.   A. Praetorius, J. Labille, M. Scheringer, A. Thill, K. Hungerbuhler and J. Y. Bottero, *Environmental Science & Technology*, 2014, **48**, 10690-
380   10698.
381 16.   P. Zhang, X. He, Y. Ma, K. Lu, Y. Zhao and Z. Zhang, *Chemosphere*, 2012, **89**, 530-535.
382 17.   G. V. Lowry, B. P. Espinasse, A. R. Badireddy, C. J. Richardson, B. C. Reinsch, L. D. Bryant, A. J. Bone, A. Deonarine, S. Chae, M. Therezien, B.
383   P. Colman, H. Hsu-Kim, E. S. Bernhardt, C. W. Matson and M. R. Wiesner, *Environmental Science & Technology*, 2012, **46**, 7027-7036.
384 18.   M. Von Smoluchowski, *Z. Physik. Chem.* , 1917).], **92**.
385 19.   L. Barton, M. Therezien, M. Auffan, J.-Y. Bottero and M. Wiesner, *Environmental Engineering Science*, 2014, **31**, 421-427.
386 20.   M. Therezien, A. Thill and M. R. Wiesner, *Science of The Total Environment*, 2014, **485–486**, 309-318.
387 21.   J. Labille, C. Harns, J.-Y. Bottero and J. Brant, *Environmental Science & Technology*, 2015, **in press**.
388 22.   D. Zhou, A. I. Abdel-Fattah and A. A. Keller, *Environmental Science & Technology*, 2012, **46**, 7520-7526.
389 23.   J. Zhao, F. Liu, Z. Wang, X. Cao and B. Xing, *Environmental Science & Technology*, 2015, **49**, 2849-2857.
390 24.   M. F. Brigatti, E. Galan and B. K. G. Theng, in *Handbook of Clay Science. Developments in Clay Science*, eds. F. Bergaya, G. K. B. Theng and G.
391   Lagaly, Elsevier, Amsterdam, 2006, vol. 1, pp. 19–86.
392 25.   E. Tombacz and M. Szekeres, *Applied Clay Science*, 2006, **34**, 105–124.
393 26.   M. Sayed Hassan, F. Villieras, A. Razafitianamaharavo and L. Michot, *Langmuir*, 2005, **21**, 12283-12289.
394 27.   O. Söhnel and J. Garside, in *Basic Principles and Industrial Applications*, ed. Butterworth-Heinemann, Boston, 1992, p. 149.
395 28.   R. M. Smith and A. E. Martell, ed. NIST, 2004, vol. 8.
396 29.   A. M. Shahin, F. Grandjean, G. J. Long and T. P. Schuman, *Chemistry of Materials*, 2005, **17**, 315-321.
397 30.   J.-D. Cafun, K. O. Kvashnina, E. Casals, V. F. Puntes and P. Glatzel, *ACS Nano*, 2013, **7**, 10726-10732.
398 31.   G.-A. Paffenhöfer and K. D. Lewis, *Journal of Plankton Research*, 1990, **12**, 933-946.
399 32.   U. Sommer and F. Sommer, *Oecologia*, 2006, **147**, 183-194.
400 33.   X. Zhu, Y. Chang and Y. Chen, *Chemosphere*, 2010, **78**, 209-215.
401 34.   M. Auffan, D. Bertin, P. Chaurand, C. Pailles, C. Dominici, J. Rose, J.-Y. Bottero and A. Thiery, *Water research*, 2013, **47**, 3921-3930.
402 35.   E. Artells, J. Issartel, M. Auffan, D. Borschneck, A. Thill, M. Tella, L. Brousset, J. Rose, J.-Y. Bottero and A. Thiery, *PlosOne*, 2013, **8**, e71260.
403 36.   J. B. Graham, *American Zoologist*, 1990, **30**, 137-146.

404